

Diblock Copolymer Reinforced Interfaces between Amorphous Polystyrene and Semicrystalline Polyethylene

J. J. Benkoski, P. Flores, and E. J. Kramer*

Materials Department, University of California, Santa Barbara, California 93106

Received January 5, 2003

ABSTRACT: The effects of molecular architecture on the fracture properties of semicrystalline polymers were probed at diblock copolymer-reinforced interfaces between polystyrene (PS) and polyethylene (PE). The PE used for this study was a model ethylene–butene copolymer which was chosen for its compatibility with hydrogenated 1,4-polybutadiene. This compatibility allowed the use of hydrogenated poly(styrene-*b*-1,4-tetradeuteriobutadiene) as the block copolymer. For a series of these diblock copolymers, the areal chain density (Σ) and the molecular weight of the PE block (M_n) were varied systematically to observe their effects on the interfacial fracture energy (G_c). At low Σ , G_c stayed relatively constant, and was roughly 1 J/m². Above a critical value of Σ , the fracture energy climbed rapidly. This critical value decreased with increasing M_n . The detection of deuterium on the fracture surfaces indicated that pullout of the PE block was the predominant failure mechanism when $M_n \leq 30$ kg/mol. Only when the molecular weight of the PE block reached 85 kg/mol was failure by chain scission observed. Since the entanglement molecular weight of PE is approximately 1 kg/mol, interfacial reinforcement does not appear to depend on the formation of entanglements for this system. The critical M_n coincides instead with the point at which the root-mean-square end-to-end length of the PE block exceeds the long period of the PE crystal lamellae (L). The preceding observation is consistent with the decrease in G_c with increasing L near the critical molecular weight.

Introduction

Polyethylene. Polyethylene (PE) leads all materials in world annual production by volume.¹ Its popularity is driven by several key properties, which include toughness, ease of processing, chemical resistance, and low cost. Its uses are similarly diverse and range from storage containers to cut-resistant surgical gloves. Despite its importance as a structural material, the effects of chain architecture on its fracture properties are poorly understood. Much more is known about the molecular details of fracture in glassy polymers. In contrast, the molecular mechanisms of fracture in semicrystalline polymers are often obscured by the complex relationship between their microstructure and mechanical properties. Though this characteristic is one of their most useful features, it makes them less attractive as model systems.

PE has the simplest repeat unit of all polymers, with only CH₂ groups along its backbone. Its chains crystallize in a fully extended conformation. It forms an orthorhombic unit cell with dimensions 7.41 × 4.94 × 2.55 Å.² Because PE chains are highly entangled in the melt, the kinetics of crystallization rarely permit the formation of large, perfect crystals. Instead, its crystals take the form of either folded chain lamellae or fringed micelle crystallites. The latter form is less common and results only from rapid quenching or extensive chemical irregularity along the chains.³

The unbranched form of polyethylene can achieve crystallinities greater than 90%. Most commercial polyethylenes, however, are less crystalline. One such material is known as linear low-density polyethylene (LLDPE). LLDPE is synthesized by copolymerizing ethylene with an α -olefin that produces short side

groups. These side groups disrupt crystal formation, resulting in a large fraction of amorphous material. As the glass transition temperature of PE is well below room temperature, these amorphous regions are rubbery under ambient conditions.^{4–6} The loss in crystallinity and the corresponding decrease in Young's modulus are compensated by an increase in toughness.

A material similar to LLDPE is hydrogenated 1,4-polybutadiene (h-PBD). The starting h-PBD is synthesized by the anionic polymerization of 1,3-butadiene in a nonpolar solvent, such as cyclohexane. Under normal reaction conditions, 1,2-addition is unavoidable. Under the best reaction conditions, the polymerization produces around 10% 1,2-additions.^{7,8} What results is a linear polybutadiene with only a small fraction of ethyl branches. When this polymer is fully hydrogenated, it is nearly identical to poly(ethylene-*r*-butene). The advantages of synthesizing LLDPE in this manner, compared to random copolymerization, is the ability to produce a nearly monodisperse polymer and the ability to synthesize block copolymers.

Semicrystalline Polymer Interfaces. The extensive use of semicrystalline polymers is due, in part, to the ability to control their properties. This range of properties can be extended even further through alloying or surface modification. Nevertheless, both procedures are limited by the difficulty of forming strong interfaces with semicrystalline polymers. Although many methods for improving the fracture energy of polymer–polymer interfaces are currently available, their application to semicrystalline polymers is not straightforward. The main problem is achieving cocrystallization between two different polymers. While coentanglement occurs readily for miscible polymer chains, cocrystallization does not. This fact is particularly important when the amorphous phase is rubbery, because even when entanglements do form across the

* To whom correspondence should be addressed. E-mail: edkramer@mrl.ucsb.edu.

interface, they can slide apart with little resistance. Reinforcement can only occur when entanglements are trapped between pairs of crystallites or when individual chains can anchor themselves in crystals on both sides of the interface. The use of block copolymers is ideally suited for achieving the latter condition. In addition to being able to control the degree of mechanical coupling, block copolymers can also be used to control the blend morphology.

The use of diblock copolymers has been studied extensively at interfaces between isotactic polypropylene (iPP) and polyamide 6 (PA6).^{9–13} For this industrially important system, the diblock copolymers were formed in situ via reactive end groups on each type of chain. The fracture energy (G_c) increased up to 700 J/m² under optimized conditions.⁹ Similar increases in peel strength were observed when polystyrene-*b*-hydrogenated butadiene copolymers were added to interfaces between PS and PE.¹⁴ Thick layers of high molecular weight copolymer were even found to result in cohesive failure through the PE beam. The G_c of PE interfaces with glass also increased greatly when polyethylene chains were grafted to the glass surface.¹⁵

When an AB diblock copolymer is placed at a molten interface between its parent homopolymers, the A block diffuses into polymer A, and the B block diffuses into polymer B. This penetration allows the copolymer to transfer stress across the interface. When the block lengths are held constant, the magnitude of this stress is proportional to Σ , the areal density of block copolymer chains. If the force transferred per chain is large enough, then crazes will be sustained across the interface above a critical value of Σ . This value is denoted by Σ_c when the chains fail by scission and by Σ^\dagger when they fail by pullout. Both transitions are accompanied by an abrupt increase in the fracture energy. Another critical value of Σ exists, Σ_{sat} . Above this density, the block copolymers will be expelled from the interface due to the entropic penalty of chain stretching. Additional copolymer will pinch off to form micelles, cylinders, or lamellae depending on the molecular weight ratio of the two blocks. Washiyama et al. found that lamellar overgrowths could form weak boundary layers at the interface.¹⁶ The consequence of Σ_{sat} is that placing additional diblock copolymer at an interface does not improve the interfacial fracture energy without limit.

The dependence of stress transfer on the degree of polymerization of each block, N , is more complicated. For glassy polymers, the force transferred by an unentangled block during pullout is directly proportional to its degree of polymerization. The stress is given by $\Sigma f_{\text{mono}} N$, where f_{mono} is the static coefficient of friction per mer.^{17,18} Once a block becomes entangled in a glassy matrix, it cannot be removed by pullout. Rather, it will fail by chain scission and transfer a maximum force equal to that needed to break a carbon–carbon bond (f_b). The stress transferred when scission is the failure mechanism is therefore given by Σf_b .^{17,18} The transition from chain pullout to chain scission typically occurs when the molecular weight of each block exceeds its respective entanglement molecular weight (M_e). Since the load transferred during scission greatly exceeds that of pullout, Σ_c is generally much lower than Σ^\dagger .

The above dependence of interfacial stress transfer on the copolymer molecular weight only holds for glassy polymers. Because they lack a microstructure, the only

critical parameter is the entanglement molecular weight. The stress transfer of a semicrystalline block, on the other hand, can be a function of the level of cocrystallization, crystallite thickness, interlamellar thickness, or the supermolecular structure.^{19,20} Collectively, these parameters comprise the microstructure of the polymer and vary with the thermomechanical history. The importance of this history means that processing variables such as cooling rate and annealing time must be controlled in addition to physical parameters such as N and Σ .

Boucher et al., found that G_c for the PA6/iPP system obeyed the same dependence on Σ as glassy systems so long as the plastic deformation zones remained localized Dugdale-type zones.^{10,11} However, they found significant deviations from this behavior when the fracture samples were annealed above the melting point of the PA6. For such annealing temperatures, they observed the appearance of the iPP β crystalline phase. They also noted that diffuse deformation zones began to form in addition to the main cavitation plastic zone. Subsequent transmission electron microscopy (TEM) studies by Kalb et al. could not identify a clear relationship between the change in mechanism and the presence of the β phase.¹³

Deviations from the behavior of glassy polymer–polymer interfaces were also noted by Chaffin et al.²¹ They synthesized an ABA triblock copolymer of hydrogenated polybutadiene in which the A blocks had 7% 1,2-addition and the B blocks had 88% 1,2-addition. This copolymer was added to blends between PE and isotactic polypropylene (iPP). The A blocks were miscible with PE and the B blocks were miscible with iPP. Although the B blocks were compatible in the melt, they could not cocrystallize with iPP. The result was a rubbery amorphous phase on the iPP side of the interface. The addition of the triblock copolymer to PE/iPP blends therefore reduced the elongation to failure, decreased the toughness, and resulted in interfacial fracture.

The above examples illustrate the large number of variables that can affect the behavior of interfaces involving semicrystalline polymers. The goal of this study, then, is to identify the most important factors by examining the effects of placing poly(styrene-*b*-1,4-tetradeuteriobutadiene) at an interface between polystyrene and poly(ethylene-*r*-butene). The use of this model system will enable the observation of the change in interfacial fracture energy as a function of the length of the semicrystalline block and the areal chain density. The effects of microstructure on the fracture energy will also be studied by changing the cooling rate of the sample from the melt. To study the dynamics of the system, the experiments will also probe the influence of the crack growth rate and temperature on the interfacial fracture energy.

Experimental Section

Materials Poly(styrene-*b*-1,4-tetradeuteriobutadiene) was synthesized anionically from 1,1,4,4-tetradeuteriobutadiene and styrene. 1,1,4,4-Tetradeuteriobutadiene was obtained by decomposing butadienyl-2,2,5,5-*d*₄ sulfone (Aldrich) at 180 °C under a constant nitrogen flow. After the gaseous products were bubbled through a 10 wt % NaOH solution to remove the SO₂, the product was collected over a bath of dry ice and 2-propanol. Next, it was purified by successive distillation from dibutylmagnesium (Aldrich) and *n*-butyllithium (Aldrich). Styrene (Aldrich) was likewise purified by successive distillation from CaH₂ (Aldrich) and dibutylmagnesium.

Table 1. Diblock Copolymer Molecular Weights

name	M_n (kg/mol)			PDI total
	total	PS	PE	
PS33-dPE3	36 700	33 400	3300	1.03
PS45-dPE7	52 400	45 000	7400	1.13
PS40-dPE30	69 600	40 100	29 500	1.02
PS50-dPE85	136 000	50 500	85 500	1.14

Table 2. Physical Properties of the Two Homopolymers

material	T_g , °C	T_m , °C	E, MPa	σ_c , MPa	σ_y , MPa
polystyrene	100		3000	55	
polyethylene	-25	100	86		5.5

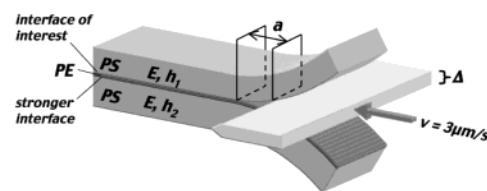
To minimize 1,2-addition in the butadiene block, the polymerizations were performed in nonpolar cyclohexane. Water and gaseous impurities were removed from the cyclohexane by distilling it from an orange poly(styryllithium) solution. To the pure cyclohexane was added the *sec*-butyllithium initiator, the concentration of which had been determined using the double titration technique of Gilman and Cartledge.²² All steps were performed at 40 °C under constant stirring. Styrene was added first, allowing 6 h for the monomer to be consumed. Next, 1,1,4,4-tetradeuteriobutadiene was added, and the polymerization was allowed to run to completion overnight. Finally, the reaction was quenched with degassed butanol and the polymer precipitated into 2-propanol.

To convert the unsaturated block of poly(1,4-tetradeuteriobutadiene) into a linear low density polyethylene, the diblock copolymer underwent a partial hydrogenation. Wilkinson's catalyst was prepared by adding 0.8 g/L each of chlorotris-(triphenylphosphine)rhodium(I) and triphenylphosphine to dry toluene. Also prepared was a 10 wt % solution of the polymer in dry toluene. When both mixtures were fully dissolved, they were added in a 1:4 volume ratio to a high-pressure vessel, and the vessel was purged with nitrogen. The solution was then heated to 100 °C under vigorous stirring. Exposure of the solution to hydrogen gas at 0.62 MPa was sufficient to drive the hydrogenation forward. The reaction was allowed to proceed for 24 h to ensure 100% hydrogenation of the 1,4-tetradeuteriobutadiene block. At the conclusion of the reaction, all traces of the catalyst were removed from the polymer by precipitating it in 2-propanol three times. The hydrogenation was then evaluated by dissolving the copolymer in $CDCl_3$ and taking nuclear magnetic resonance (NMR) spectra with a Bruker AVANCE200 NMR spectrometer. The removal of the unsaturated bonds in the polymer was verified by the disappearance of the corresponding NMR peaks.

The molecular weights and polydispersities of each diblock copolymer were determined using size exclusion chromatography (SEC) with THF as the mobile phase. The SEC data are shown in Table 1. NMR analysis of the hPBD determined that the reaction proceeded with 91% 1,4-addition. This percentage gives an average of 23 ethyl branches for every 1000 main chain carbon atoms.

The bulk polymers used for mechanical testing were polystyrene (PS) and poly(ethylene-*r*-butene) (PE). PS was obtained from Aldrich with M_n equal to 200 kg/mol and M_w equal to 400 kg/mol. A 70 μ m thick film of PE was obtained from Exxon having M_n equal to 31.7 kg/mol and M_w equal to 68.6 kg/mol. The polymer contained 25 ethyl branches per 1000 C atoms according to NMR analysis. Data on the mechanical properties of both polymers are given in Table 2.

Asymmetric Double Cantilever Beam. All fracture energy measurements were made using the asymmetric double cantilever beam (ADCB) technique, as illustrated in Figure 1. The ADCB method measures the interfacial fracture energy (G_c) by equating the energy needed to create two new surfaces with the elastic energy stored in the top and bottom beams. Knowing the thickness of the wedge (Δ), the stiffness of the beams (E), the thicknesses of the beams (h), and the crack

**Figure 1.** Asymmetric double cantilever beam schematic illustrating how only one PS/PE interface is tested.

length (a) allows one to determine the critical strain energy release rate (fracture energy) of the interface:

$$G_c = \frac{3\Delta^2 E_1 h_1^3 E_2 h_2^3}{8a^4} \times \frac{E_1 h_1^3 C_2^2 + E_2 h_2^3 C_1^2}{(E_1 h_1^3 C_2^3 + E_2 h_2^3 C_1^3)^2} \quad (1)$$

where $C_1 = 1 + 0.64h/a$.

The ADCB technique is ideally suited for interfacial studies. Because crack growth at an interface typically involves both mode I (opening) and mode II (sliding) components, the analysis can be more complicated than for a bulk material. Often, cracks will deviate toward the more compliant material and result in an artificially high measurement of fracture energy. The ADCB technique addresses this problem by controlling the ratio of the opening and shear mode stress intensity factors, K_I and K_{II} . This ratio is referred to as the mode mixity, and is represented by the phase angle, ψ :

$$\psi = \tan^{-1} \left(\frac{K_{II}}{K_I} \right) \quad (2)$$

The mode mixity is determined by the relative thickness and compliance of the two beams in the sample. The thickness ratio of the two beams can therefore be adjusted so that failure occurs primarily in opening mode regardless of the compliance ratio. It also makes it possible to pin the crack against the material with the higher yield stress. The crack is therefore guided along the interface, and a true measure of the interfacial fracture energy is obtained.

Because of the low elastic modulus of PE, and the difficulty of achieving plane strain conditions, it was not suitable for use as an elastic beam. This problem was avoided by backing a thin (70 μ m) film of PE with a PS beam, as shown in Figure 1. Although this geometry resulted in two PS-PE interfaces, only one was tested. The isolation of a single interface was achieved by making one much stronger than the other. The stronger interface was reinforced using a thick layer of the highest molecular weight diblock copolymer in this study. It consisted of a 45 kg/mol PS block and a 90 kg/mol PE block (PS45-PE90). An areal chain density of 0.2 chains/nm² provided the maximum reinforcement, and ensured the integrity of the interface during all fracture experiments. The PE block for this copolymer was not labeled with deuterium.

The 70 μ m PE film was therefore coated on both sides with diblock copolymer. On one side was placed 0.2 chains/nm² of the PS45-PE90 copolymer, while on the other side was placed the copolymer of interest. Both were deposited by spin casting from toluene solution at 70 °C. Cast at a constant speed of 3000 rpm, the diblock copolymer coating had its thickness adjusted by changing the concentration of the solution. All four deuterated diblock copolymers were tested, with their areal chain densities controlled by varying the thickness of the coating.

The ADCB specimens were made by first molding a pair of PS plaques in a hot press at 200 °C. The two plaques measured 50 \times 70 \times 2.4 mm and 50 \times 70 \times 2.1 mm, respectively. Between the plaques was placed the PE film coated with diblock copolymer. The trilayer sandwich was then welded in a hot press under light pressure at 160 °C for 2 h. Upon removal from the press, the samples were quenched to room temperature in 2.7 min unless otherwise stated. Finally, the

plaques were diced into individual samples using a slow-speed diamond saw. The final sample dimensions were $40 \times 8 \times 4.6$ mm.

The beam thicknesses were chosen in order to provide the minimum fracture energy. The optimum ratio had been determined previously by testing a set of specimens coated with 0.2 chains/nm² of the PS40-dPE30 copolymer. The fracture energy was then measured as a function of thickness ratio. The 2.1:2.4 ratio, which placed the fracture plane between the PE and the thinner beam, corresponds to $\psi = -5.4^\circ$, as calculated by the method of Hutchinson and Suo.²³ Note that the PE film was sufficiently thin that its elastic properties and thermal mismatch could be ignored for this analysis.²⁴

Six samples were tested for each data point, with up to 30 measurements taken per sample. Multiple measurements were taken by driving the razor blade into the interface at 3 $\mu\text{m/s}$ and capturing the images at regular intervals to a computer. Crack lengths were then measured using NIH Image software.

Forward Recoil Spectrometry. The amount of deuterated material on each fracture surface was measured using forward recoil spectrometry (FRES). This allowed the determination of the total areal chain density of diblock copolymers at the interface, and the relative amount of copolymer on each side of the fracture plane. The former provides a more accurate measurement than that based on ellipsometry, while the latter can be combined with the fracture energy data to determine the failure mechanism. Since all PS blocks used in this experiment were roughly double the entanglement molecular weight, they were assumed to remain firmly embedded in the PS homopolymer for all cases. This assumption made it possible to determine whether the PE blocks failed by pullout or scission. Details of this technique can be found in refs 17, 25, and 26.

Transmission Electron Microscopy. Transmission electron microscopy (TEM) was used both to assess the impact of the diblock copolymers on the structure of the interfaces and to observe the changes in the PE microstructure as a function of cooling time. TEM samples were prepared from unused ADCB specimens by first trimming 200 μm trapezoidal areas with a diamond blade at -185°C . The samples were then stained by immersion in aqueous RuO₄ solution for 16 h. From the interfacial region, 70 nm thick slices were microtomed using a Leica Ultracut UCT at room temperature. Finally, bright-field TEM images were captured using a JEOL 2000FX electron microscope.

Light Optical Microscopy. Due to the optical clarity of the PS beams, crack growth could be monitored in situ using a light optical microscope in reflection mode with crossed polarizers. The experiments were performed by slowly driving a razor blade into the interface while the specimens were loaded on top of the microscope stage. A computer interfaced to a Sony CCD-IRIS color video camera then captured an image to the hard drive every 5 s. All four diblock copolymers were tested, with each sample having a constant areal chain density of 0.2 chains/nm². A bare PS-PE interface was also tested for comparison.

Small Angle X-ray Scattering. Small-angle X-ray scattering (SAXS) was used to determine the long period (L) of the PE lamellae. The measurements were performed on PE films for several different sample cooling times: 2.7, 5.0, 9.5, 30, and 360 min. The bare PE films were removed from the PS plates by first dissolving away the PS in THF under constant stirring. The measurements themselves were performed using Cu K α ($\lambda = 1.542 \text{ \AA}$) radiation and a 1024×1024 Bruker HI-STAR multiwire area detector with a 1.5 m sample to detector distance. To include the proper length scale, the scattering vector (q) ranged from 0.01 to 0.15 \AA^{-1} . Here q is defined as the difference between the scattered wave vector (k) and the incident wave vector (k_0).

The two-dimensional diffraction patterns were then converted to plots of intensity vs q using the shareware program, FIT2D. After the conversion, the intensity was multiplied by a Lorentzian correction factor of $2\pi q$. The peak position in q ,

q^* , was then determined from a fit to a log-normal function of the form

$$I = I_0 + A [\exp\{-\{\ln(q/q^*)/B\}^2\}] \quad (3)$$

where I is the intensity, and I_0 , A , and B are constants. The parameter q^* is related to the lamellar long period (L) by $L = 2\pi/q^*$. Arising from the regular stacking of lamellae, L is the sum of the lamellar thickness and the width of the amorphous region separating adjacent pairs.

Dynamic Scanning Calorimetry The melting point (T_m) and enthalpy of melting (ΔH_f) were measured using dynamic scanning calorimetry (DSC). To maximize the temperature resolution, the T_m was measured using 1 mg samples of PE ramped at 2°C/min . To maximize the heat flow sensitivity, ΔH_f was determined separately from 10 mg samples that had been ramped at 10°C/min . As with the SAXS measurements, the PS had been removed previously by THF extraction. All samples were cooled from 160 to 40°C in 2.7 min.

Both T_m and ΔH_f were independent of the areal chain density or molecular weight of the diblock copolymer used to reinforce the interface. A virgin specimen of PE, which was not subject to the constraint of the PS plaques, had the same T_m and ΔH_f as well. The two values were measured to be 96.6°C and 94.5 J/g, respectively. Using a value of 288 J/g for the enthalpy of melting of a pure PE crystal,²⁷ the latter value corresponded to a crystallinity of 32.8 wt %.

Experimental Variables. The interfacial fracture energy was measured as a function of six variables: PE block molecular weight, areal chain density, PE film thickness, sample cooling time, crack growth rate, and temperature. To examine the effects of areal chain density, the cooling time was fixed at 2.7 min, the crack growth rate was fixed at 3 $\mu\text{m/s}$, and the PE film thickness was fixed at 70 μm . The tests were repeated for all four deuterated copolymers.

For the PE film thickness measurements, the cooling time was fixed at 2.7 min. The measurements were performed for the PS40-dPE30 copolymer at 0.12 chains/nm² and for the PS50-dPE85 copolymer at 0.20 chains/nm².

To test the effects of the sample cooling time, the film thickness was fixed at 70 μm . Both the PS40-dPE30 and PS50-dPE85 copolymers were tested at 0.2 chains/nm².

All four deuterated copolymers were tested as a function of crack growth rate. Their areal chain densities were as follows: PS33-dPE3 = 0.22 chains/nm², PS45-dPE7 = 0.18 chains/nm², PS40-dPE30 = 0.21 chains/nm², and PS50-dPE85 = 0.2 chains/nm². Each rate experiment was performed with a constant cooling time of 2.7 min and a PE film thickness of 70 μm .

The rate experiments were then followed by the measurement of G_c as a function of temperature for the PS40-dPE30 copolymer. For this set of tests, the cooling time was 2.7 min, the crack growth rate was 3 $\mu\text{m/s}$, the film thickness was 70 μm , and the areal chain density was approximately 0.13 chains/nm².

Results

PS33-dPE3. The interfacial fracture energy for the PS33-dPE3 copolymer as a function of Σ is represented in Figure 2. Within the scatter of the data, the fracture energy remained constant and was approximately equal to that of the bare interface. The lone exception was the slight jump at 0.20 chains/nm², which amounted to only 0.6 J/m². Not surprisingly, the FRES data indicated that 100% of the dPE block remained on the PS side of the fracture plane in all cases. Although the molecular weight of the dPE block is roughly three times larger than the entanglement molecular weight of the polyethylene, it pulled out of the PE homopolymer without causing significant energy dissipation.

PS45-dPE7. Figure 3 displays G_c as a function of Σ for the PS45-dPE7 copolymer. Unlike the previous case,

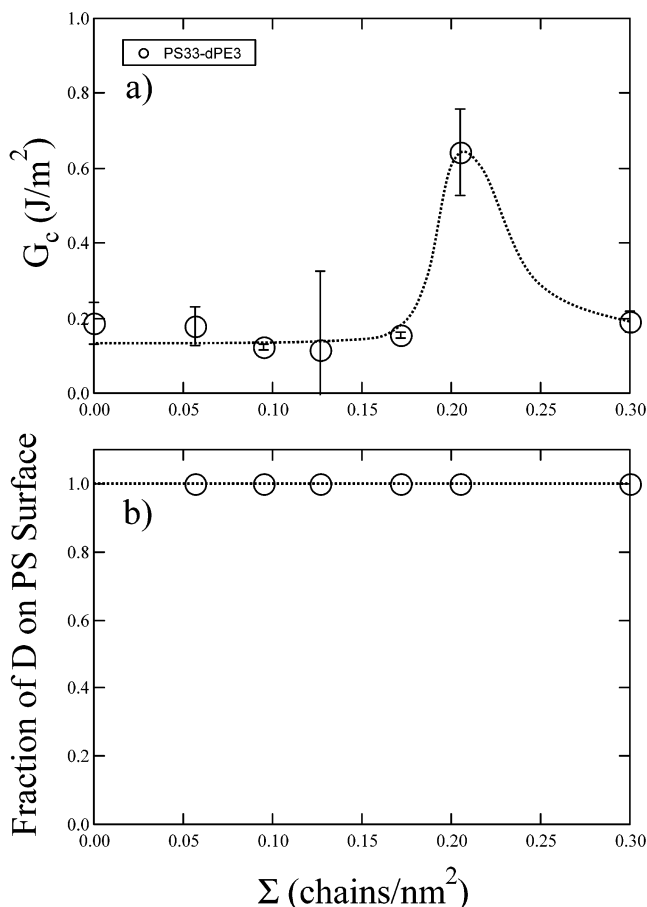


Figure 2. (a) Fracture energy plotted as a function of areal chain density for the PS33-dPE3 copolymer. (b) Fraction of deuterium on polystyrene fracture surface after fracture also plotted vs areal chain density. The dotted lines are guides to the eye.

this copolymer produced a noticeable increase in fracture energy. However, G_c failed to reach 10 J/m² at any value of Σ . The FRES data showed that the copolymers failed by pullout of the dPE block from the PE side of the interface at this molecular weight as well. Observe that no significant increase in fracture energy from the bare interface value occurred until $\Sigma \geq 0.16$ chains/nm². Observe also the maximum in fracture energy at about 0.2 chains/nm².

PS40-dPE30. The samples coated with the PS40-dPE30 diblock copolymer were the first for which crazing could be observed at higher Σ through the whitening of the PE surface after failure. The G_c vs Σ data in Figure 4 show a behavior qualitatively similar to that exhibited by the PS45-dPE7 copolymer. In this case, however, the maximum value of G_c rose to 81 J/m² at 0.2 chains/nm² and the onset of toughening appeared at a slightly lower value of 0.08 chains/nm². Despite the large-scale crazing and a PE block molecular weight 30 times larger than the PE entanglement molecular weight, this copolymer, too, failed by pullout of the PE block for all Σ . These FRES data clearly demonstrate that craze failure can occur in conjunction with chain pullout.

PS50-dPE85. Figure 5 shows the G_c vs Σ data for the PS50-dPE85 diblock copolymer. Rising to a maximum G_c of 700 J/m², the interface for this system was so strongly reinforced that the interface failed cohesively through the PE film when the areal chain density

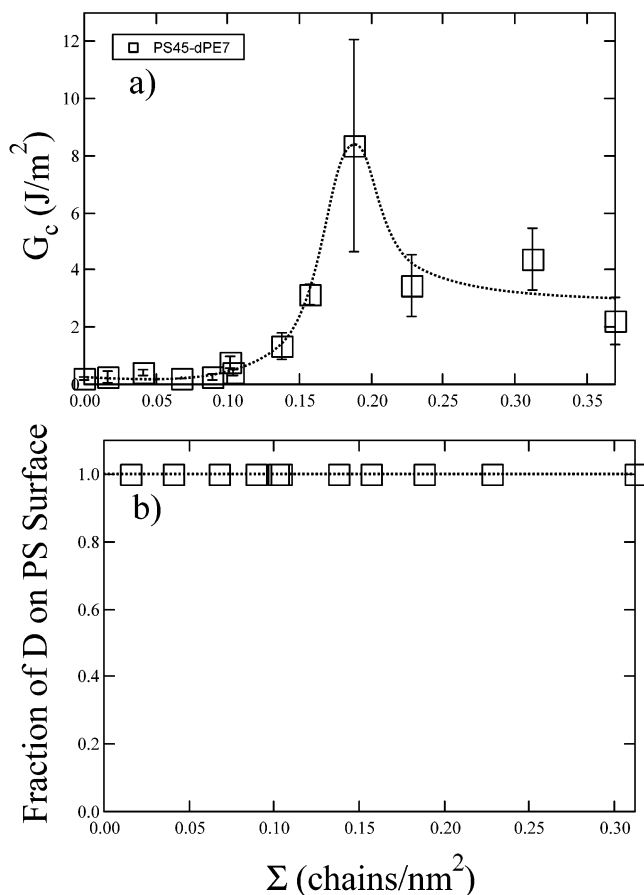


Figure 3. (a) Fracture energy plotted as a function of areal chain density for the PS45-dPE7 copolymer. (b) Fraction of deuterium on polystyrene fracture surface after fracture also plotted vs areal chain density. The dotted lines are guides to the eye.

exceeded 0.05 chains/nm². The increase in G_c began at an even lower Σ , around 0.03 chains/nm². Since FRES deuterium detection could not penetrate through the PE that remained on each fracture surface, the values of $\Sigma > 0.05$ chains/nm² had to be extrapolated from a comparison of Σ measured from FRES with the equivalent thickness of test coatings measured by ellipsometry. The thicknesses of the coatings spun cast onto silicon wafers were assumed to be equal in thickness to the coatings spun cast directly onto the PE films. The calibration showed that the maximum in G_c occurred at approximately 0.2 chains/nm², as with the other copolymers.

Figure 5b shows that the PS50-dPE85 copolymer is the first for which chain scission is observed. For those samples that did not fail cohesively, 50% of the deuterium was detected on the PE fracture surface. These FRES data suggest that the critical PE block molecular weight for chain scission has been exceeded.

Micelle and Cylinder Formation. The TEM micrographs in Figure 6 display interfaces with high areal chain densities. Like the fracture data, the images show a transition for each diblock copolymer above 0.2 chains/nm². The PS33-dPE3 and PS45-dPE7 copolymers formed micelles above this concentration, and the PS40-dPE30 and PS50-dPE85 copolymers formed disordered cylinders. In all cases, the secondary structures formed on the PS side of the interface. This location suggests that the PS block formed the outer brush for both the micelles and cylinders. Such an observation is consistent

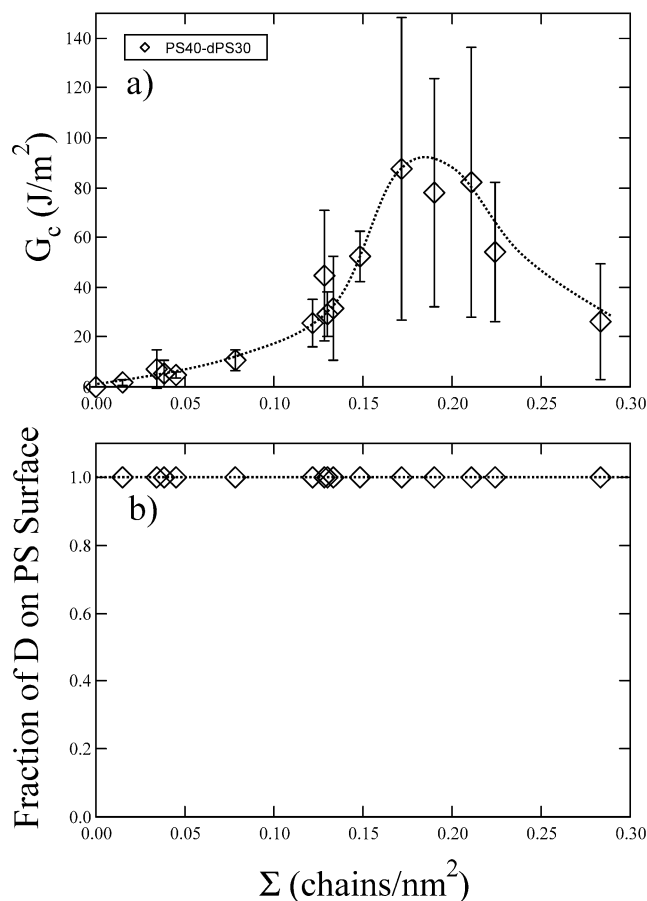


Figure 4. (a) Fracture energy plotted as a function of areal chain density for the PS40-dPE30 copolymer. (b) Fraction of deuterium on polystyrene fracture surface after fracture also plotted vs areal chain density. The dotted lines are guides to the eye.

with the fact that the PS block is longer for the PS33-dPE3, PS45-dPE7, and PS40-dPE30 copolymers. In the case of the PS50-dPE85 copolymer, it is likely that the PS block swelled selectively in toluene and that the morphology shown in Figure 6d is an artifact of the spin-coating process.

PE Film Thickness. To gauge the effects of the sample geometry on the measured interfacial fracture energies, G_c was also measured as a function of PE film thickness. In addition to a 70 μm thick film, fracture specimens were prepared with 140, 210, and 280 μm thick films. All samples from the PS40-dPE30 series were prepared with a constant areal chain density of 0.12 chains/nm². Samples from the PS50-dPE85 series were prepared with an areal chain density of 0.2 chains/nm². Within the scatter of the data, the fracture energy was independent of film thickness, as shown in Figure 7. This result suggests that the plastic zones in this study are small compared to the thickness of the 70 μm thick film and that the interfacial fracture energy is insensitive to this range of plastic constraint.

Cooling Time. Samples were cooled at several different rates from 160 to 40 $^{\circ}\text{C}$. Since the cooling rates were not linear, the cooling times are reported. The times are as follows: 2.7, 5.0, 9.5, 30, and 360 min. To isolate this variable, the areal chain density was held constant at 0.2 chains/nm² for both the PS40-dPE30 and PS50-dPE85 copolymers. The PE film thickness was fixed at 70 μm , and the crack growth rate was held at 3 $\mu\text{m/s}$. The interfacial fracture energy is plotted as a

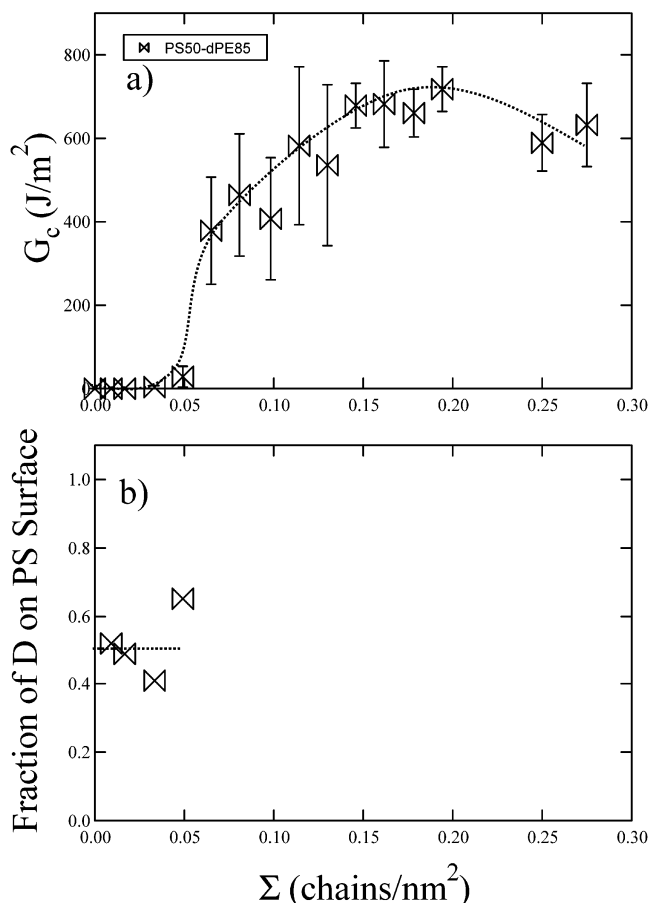


Figure 5. (a) Fracture energy plotted as a function of areal chain density for the PS50-dPE85 copolymer. (b) Fraction of deuterium on polystyrene fracture surface after fracture also plotted vs areal chain density. The dotted lines are guides to the eye.

function of cooling time in Figure 8. Observe that the fracture energy of the PS40-dPE30 samples fell sharply as the cooling time exceeded 10 min. The fracture energies of the PS50-dPE85 samples, in contrast, were not affected by the cooling rate.

Across this range of cooling times, the lamellar long period (L) changed from 14.6 nm at 2.7 min to 15.9 nm at 360 min, as shown in Table 3. These dimensions can be compared to the root-mean-square end-to-end length (R) and radius of gyration (R_g) of the PE blocks in Table 4. The outward shift in L can be observed by the inward shift of q^* depicted in Figure 9. Notice the width of the peaks. Their relative breadth indicates a fairly broad distribution for the lamellar thickness and spacing under these conditions. The TEM micrographs in Figure 10 also depict the coarsening of the microstructure with longer cooling times.

Crack Growth Rate. Crack growth rate experiments were performed for all four diblock copolymers with a PE film thickness of 70 μm and a cooling time of 2.7 min. The areal chain densities were equal to 0.2 ± 0.02 chains/nm². Five crack growth rates were tested in all: 3, 47, 147, 236, and 334 $\mu\text{m/s}$. The results are given in Figure 11. Notice that both the PS33-dPE3 and PS45-dPE7 copolymers can be fit using a power law relationship of the form $G_c = m(da/dt)^n$, with $n = 0.4$. For the PS40-dPE30 copolymer, only the first three data points follow this 0.4 power law relationship. The last two points appear to increase more slowly with da/dt , and so are not included in the fit. At these higher rates,

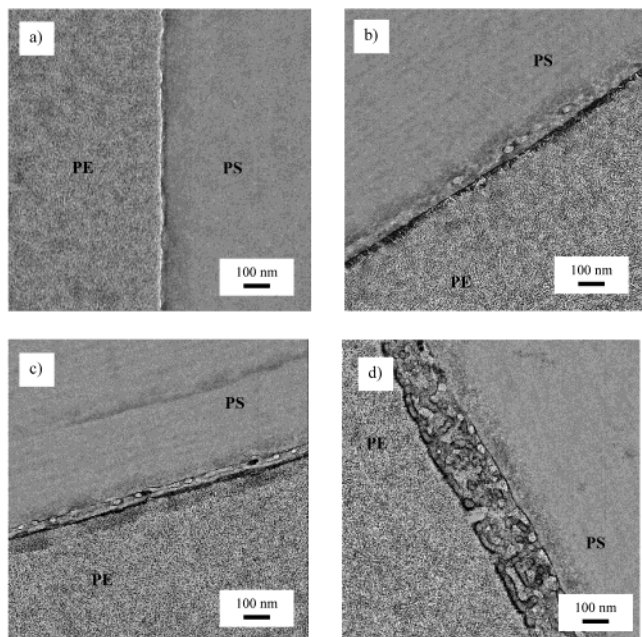


Figure 6. TEM images of (a) an interface reinforced with the PS40-dPE30 diblock copolymer at an areal density of 0.18 chains/nm², (b) micelles at an interface reinforced with 0.23 chains/nm² of the PS45-dPE7 copolymer, (c) a single layer of disordered cylinders at an interface reinforced with 0.28 chains/nm² of the PS40-dPE30 copolymer, and (d) a thick layer of disordered cylinders at an interface reinforced with 0.28 chains/nm² of the PS50-dPE85 copolymer.

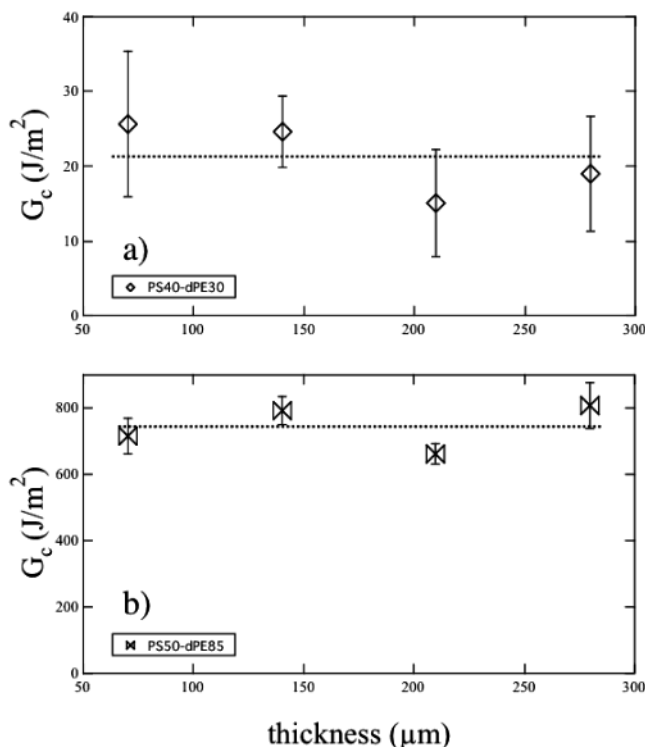


Figure 7. Interfacial fracture energy plotted as a function of thickness for the (a) PS40-dPE30 and (b) PS50-dPE85 copolymer at an areal chain density of 0.12 chains/nm² and a crack growth velocity of 3 μm/s. The dotted lines are guides to the eye.

Figure 12 shows a monotonic rise in the fraction of deuterium on the PE fracture surface from 0 to 15%. This trend indicates the beginning of the transition from chain pullout to scission. The PS50-dPE85 copolymer,

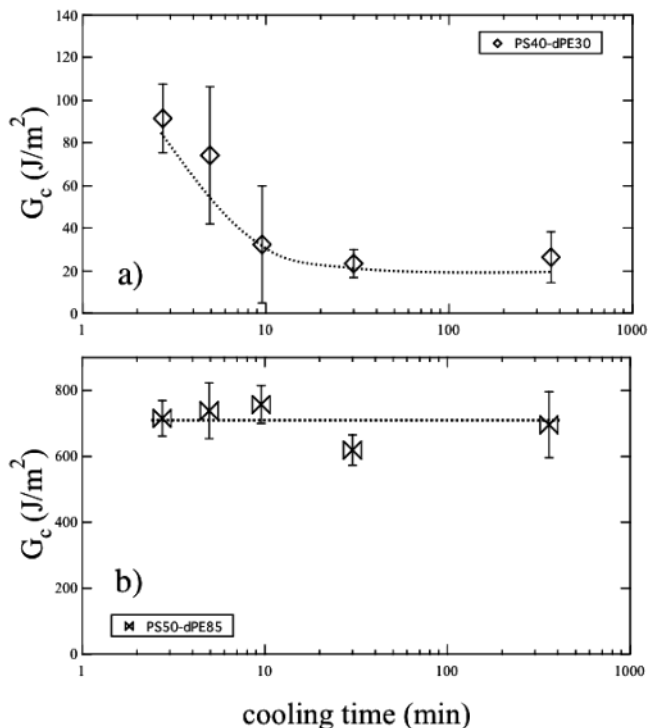


Figure 8. Interfacial fracture energy plotted as a function of sample cooling time from 160 to 40 °C for the (a) PS40-dPE30 and (b) PS50-dPE85 copolymers at an areal chain density of 0.2 chains/nm² and a crack growth velocity of 3 μm/s. The dotted lines are guides to the eye.

Table 3. SAXS Data Showing the Effects of the Cooling Time on the Long Period of the PE Lamellae

cooling time, min	q^* , nm ⁻¹	L , nm
2.8	0.430	14.6
5.0	0.424	14.8
9.5	0.422	14.9
30	0.417	15.1
360	0.394	15.9

Table 4. Root Mean Square End-to-End Length of PE Block for Each Diblock Copolymer

diblock copolymer	R , nm	R_g , nm
PS30-dPE3	6.32	2.58
PS45-dPE7	9.46	3.86
PS40-dPE30	18.9	7.71
PS50-dPE85	32.2	13.1

in contrast to the other copolymers, showed no rate dependence. Neither did it exhibit any chain pullout, as these samples failed cohesively through the PE film. This result indicates that the G_c of the bulk PE is not significantly rate dependent over this range of crack growth rates.

Temperature. G_c is recorded as a function of temperature for the PS40-dPE30 copolymer in Figure 13. The temperature ranges only from room temperature to 60 °C due to the fact that the PS beams underwent significant viscoelastic creep above this temperature. Over the range of temperatures tested, G_c appears to be constant.

Fracture Surfaces. Figure 14 includes several representative micrographs of PS-PE crack fronts. The rough appearance of the PE surfaces demonstrates that plastic deformation occurred in nearly all samples. In particular, the PS33-dPE3 sample tested at a crack growth rate of 14 μm/s showed evidence of surface

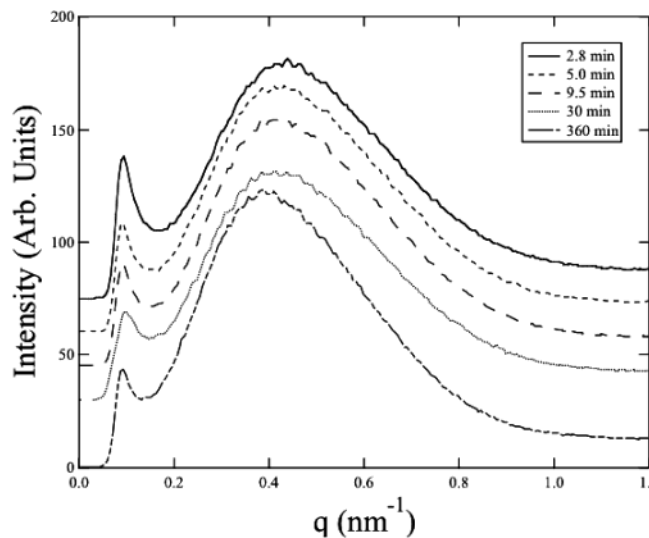


Figure 9. Small-angle X-ray scattering intensity plotted as a function of q . The curves are shifted along the y -axis for clarity.

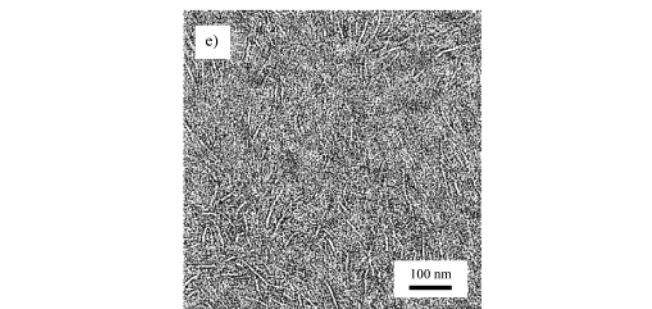
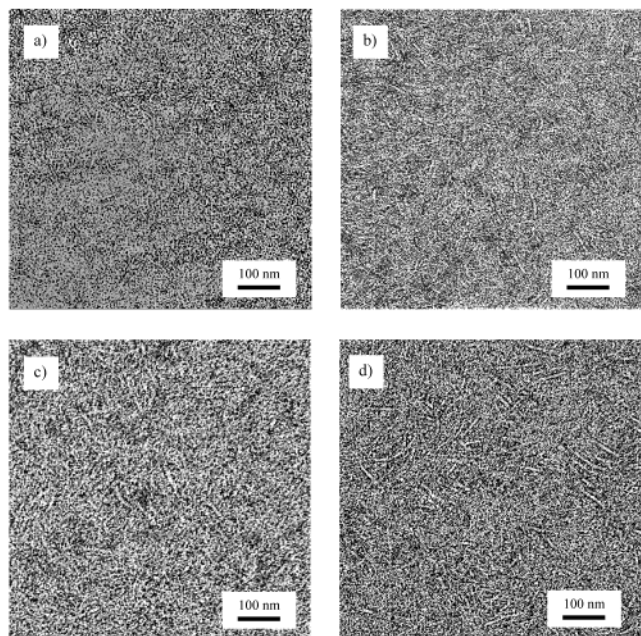


Figure 10. TEM images of bulk PE cooled from 160 to 40 °C in (a) 2.7, (b) 5.0, (c) 9.5, (d) 30, and (e) 3600 min.

roughening (Figure 14b). This observation was surprising, for the fracture energy of this particular sample was less than 1 J/m². For verification of the surface roughening, compare Figure 14b with the bare interface in Figure 14a, where multiple interference fringes are visible because of the smooth fracture surfaces. The absence of interference fringes in the remaining micro-

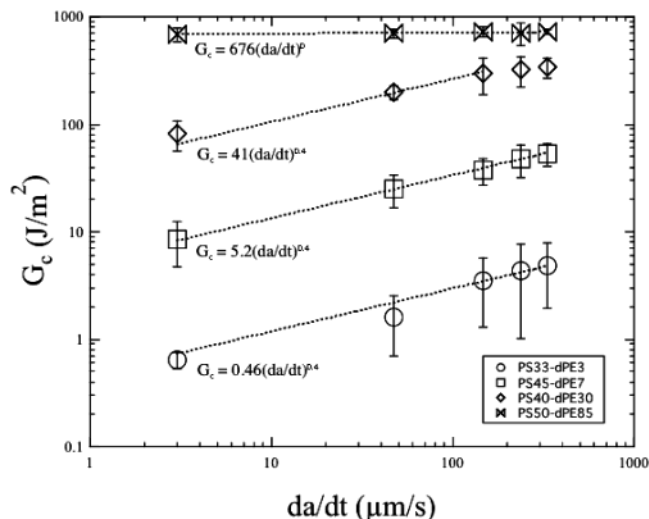


Figure 11. Log-log plot of interfacial fracture energy as a function of crack growth rate for all copolymers at an areal chain density of 0.2 chains/nm². Dotted lines are best fits using a power law relationship.

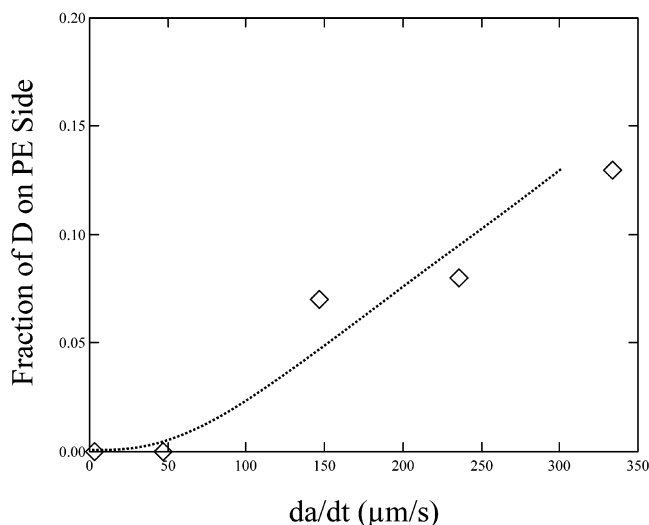


Figure 12. Fraction of deuterium on PS fracture surface as a function of crack growth rate for the PS40-dPE30 copolymer. The dotted line is a guide to the eye.

graphs indicates that at least some surface roughening occurred during crack propagation.

Although crazing is generally not observed in PS below a G_c of 10 J/m², the visual evidence suggests that crazing occurs in PE at lower values of G_c . Crazing first appears in Figure 14c, when the measured fracture energy was approximately 3.4 J/m². While surface roughening was apparent in Figures 14b–e, the nature of the deformation in Figure 14b appears to be qualitatively different than that seen in Figures 14c–e. $G_c \sim 3$ J/m² will therefore serve as a conservative lower limit for onset of crazing.

Discussion

Crazing. The most distinctive feature of the G_c vs Σ curves was the abrupt increase in the fracture energy that occurred over intermediate values of Σ . In the polystyrene–poly(2-vinylpyridine) (PS–PVP) system, such a sharp increase was only observed in connection with the onset of crazing. As the micrographs in Figure 14 showed, the onset of crazing occurred in the PE film

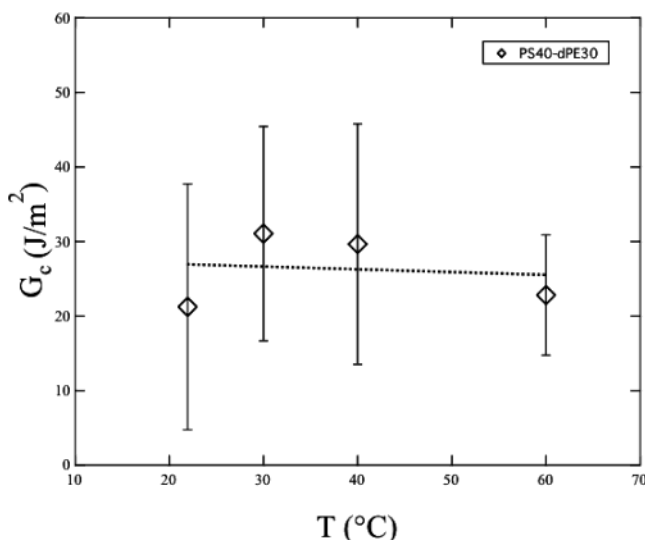


Figure 13. Plot of fracture energy vs temperature for the PS40-dPE30 copolymer at an areal chain density of approximately 0.13 chains/nm² and a crack growth rate of 3 μm/s. The dotted line is a best fit through the data.

around $G_c \sim 3 \text{ J/m}^2$. The discontinuities in Figures 3–5, therefore, indicate the transition between fracture with no crazing and fracture with crazing. What is interesting about the transition in this system is that chain failure occurs almost exclusively by pullout. Crazing in PS–PVP samples, on the other hand, occurred predominantly when the diblock copolymer chains failed by scission.¹⁷

In contrast to the glassy PS–PVP system, the deforming phase in the current system (PE) has a much lower crazing stress (σ_c). The yield stress (σ_y) for the PE used in this study is approximately 5.5 MPa according to the ASTM D-882 standard. Although the triaxial stress state during craze formation entails a slightly higher value for σ_c , one would anticipate that the two would be comparable. Contrast this PE value with the crazing stress of 55 MPa for PS. The fracture mechanism maps in Figure 15 illustrate the effect that such a dramatic decrease in σ_c would have. On these plots the y -axis represents the stress transfer due to the diblock copolymer chains (σ_d), and the x -axis represents the areal chain density. By definition, the slope of the σ_d curve is equal to the force transfer per chain. We label this force f_b when the chain undergoes scission, and f_t when the chain fails by pullout. Note that f_b is a constant, while f_t increases with molecular weight.

The purpose of the fracture mechanism map is to illustrate the relationship between the molecular parameters and the macroscopic fracture mechanism, when $\sigma_d \geq \sigma_c$, crazing occurs; otherwise, no bulk deformation takes place. In Figure 15a, σ_c is so large that the pullout stresses do not reach σ_c before Σ reaches Σ_{sat} . The value of σ_d no longer increases once the interface has saturated, so crazing only occurs when chain scission is the dominant mechanism. In contrast, the friction of chain pullout is more than adequate to induce crazing when σ_c is reduced, as shown in Figure 15b. The distinguishing feature of crazing accompanied by pullout is that Σ^\dagger decreases with increasing f_t . Compare this behavior with the results shown in Figures 2–5. In Figure 2, we see an example where crazing never occurs because $\Sigma^\dagger > \Sigma_{\text{sat}}$. From Figure 3 to Figure 4, we see a decrease in Σ^\dagger due to an increase

in the molecular weight and the corresponding f_t . Finally, Figure 5 shows the case where the chains fail by scission, and the critical areal chain density is given by $\Sigma_c = 0.033 \text{ chains/nm}^2$.

If we assume that $\sigma_d = \sigma_c$ when $\Sigma = \Sigma_c$, then we can estimate σ_c from the following equation:

$$\sigma_c = f_b \Sigma_c \quad (4)$$

With Σ_c equal to 0.033 chains/nm² and f_b given by 2 nN,¹⁷ we arrive at 66 MPa for the crazing stress. This result is unexpected given the fact that σ_c is only 55 MPa for PS.¹⁷ The crazing stress for PE is necessarily lower than that for PS because the plastic deformation occurred exclusively on the PE side. Although deuterium was found in equal amounts on both fracture surfaces, it is possible that only a fraction of the PE blocks ruptured during crack growth. If scission is assumed to have occurred at the joint between the two blocks, then the minimum fraction of chains that failed by scission is equal to 0.5. This fraction would give 33 MPa as the lower limit for the PE crazing stress.

Copolymer Saturation. With respect to the observed fracture behavior, there appears to be a correlation between micelle/cylinder formation and the decrease in G_c from its maximum value. Washiyama et al.¹⁶ observed that failure occurred through the center of such structures, indicating that they were responsible for the decrease in fracture energy. They concluded that these morphologies created weak boundary layers at the interface due to the fact that they swelled with low molecular weight homopolymer. In contrast, the FRES data from the current study indicates that the fracture plane does not deviate from the PS–PE interface. The likelihood that these structures were involved in crack propagation is further reduced by the fact that they were embedded within the hard PS phase.

Although the formation of micelles and cylinders coincides with the reduction in G_c , the experimental evidence seems to suggest correlation rather than causation. The true cause of this behavior must be taking place directly at the interface. Consider that the areal chain density at the interface between bulk PS and bulk PE should remain constant once the interface has saturated. Under equilibrium conditions, further addition of diblock copolymer should not increase the number of load-bearing chains at the interface. The G_c vs Σ plot would therefore be expected to plateau once it has reached its maximum value. Such behavior is not seen with the current system. The plots from Figures 2–5 show instead a small peak in the G_c vs Σ curve before the plateau occurs.

One possible explanation for the decrease in G_c beyond $\Sigma = 0.2 \text{ chains/nm}^2$ is that low molecular weight PE chains begin to swell the PS–PE brush at higher areal chain densities. The presence of such chains would reduce the fracture toughness locally, and allow cracks to propagate at a lower fracture energy. The relatively low molecular weight (31.7 kg/mol) and high polydispersity ($M_w/M_n = 2.16$) of the bulk PE could account for the availability of low molecular weight chains, but the idea that swelling would only become a factor for $\Sigma > \Sigma_{\text{sat}}$ is not likely.

A more probable explanation for this system is that the maximum in G_c is due to nonequilibrium conditions at the interface. Consider what happens to the local Σ at the interface between bulk PS and bulk PE once the overall Σ exceeds the saturation limit. Even though the

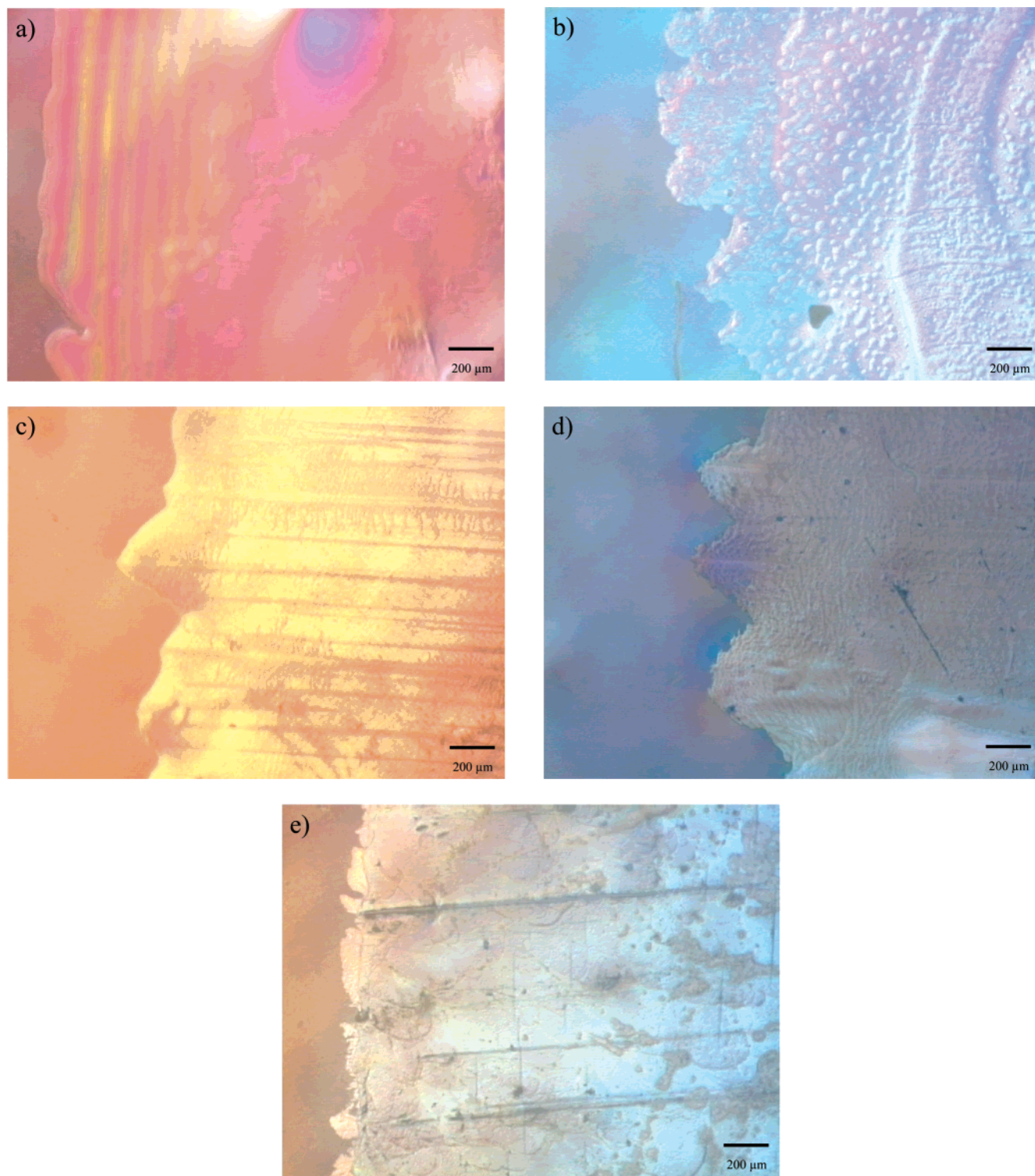


Figure 14. Optical micrograph of the crack front: (a) in an ADCB fracture specimen with a bare interface and a crack growth rate of $14 \mu\text{m/s}$ ($G_c = 0.2 \text{ J/m}^2$); (b) in a PS33-dPE3 specimen with an areal chain density of 0.20 chains/nm^2 and a crack growth rate of $14 \mu\text{m/s}$ ($G_c = 0.25 \text{ J/m}^2$); (c) in a PS45-dPE7 specimen with an areal chain density of 0.23 chains/nm^2 and a crack growth rate of $13 \mu\text{m/s}$ ($G_c = 3.4 \text{ J/m}^2$); (d) in a PS40-dPE30 specimen with an areal chain density of 0.21 chains/nm^2 and a crack growth rate of $9.3 \mu\text{m/s}$ ($G_c = 82 \text{ J/m}^2$); (e) in a PS50-dPE85 specimen with an areal chain density of 0.20 chains/nm^2 and a crack growth rate of $0 \mu\text{m/s}$ ($G_c = 717 \text{ J/m}^2$).

overall number of copolymer chains is increasing, the areal density of chains at the interface is constant. The excess diblock copolymer is consumed by the formation of micelles and cylinders. However, micelles and cylinders may not nucleate until supersaturation has occurred. Nonequilibrium concentrations greater than the saturation limit may therefore accumulate before nucle-

ation takes place. Once these secondary structures have formed, they can then provide sinks for the excess copolymer and allow the areal chain density to return to its equilibrium saturation value. Such behavior would lead to an overshoot of the stress transfer plateau and a corresponding maximum in the G_c vs Σ data. If we take Σ_{sat} equal to 0.17 chains/nm^2 and take the areal

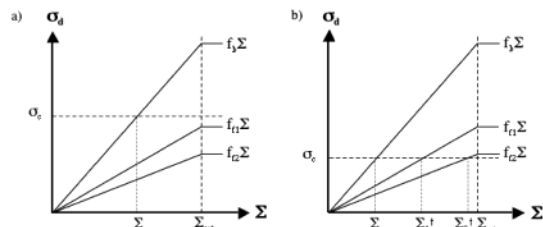


Figure 15. Fracture mechanism map for an arbitrary polymer. Craze is only possible for chains that fracture by scission in part a. For the lower crazing stress in part b, craze failure can be accompanied by either scission or pullout, and Σ^1 will decrease with increasing block molecular weight, going no lower than Σ_c .

density needed for nucleation equal to 0.2 chains/nm², then we see that the data from Figures 2–5 are not inconsistent with such a claim. Nonetheless, this hypothesis cannot be confirmed directly due to the scatter of the data.

Cocrystallization. The amorphous phase of PE is well above its glass transition point at room temperature. Without the presence of crystals, the amorphous phase would simply be a viscous melt. This portion of the material, which makes up 67% of the total structure, would not be expected to reinforce the interface greatly by way of chain friction. At the same time, it is hard to imagine chains with $M_n > 30 M_e$ failing to encounter a single entanglement. Even if crystallization were to decrease the concentration of entanglements, a material with this degree of crystallinity is not likely to decrease the concentration by more than a factor of 30. Rather, entanglements likely exist in concentrations comparable to the melt, but the chains probably disentangle readily as they do for other polymer melts with this viscosity.

The expectation that M_e should influence the performance of diblock copolymers originates in the studies of glassy polymers. Kramer et al. found that the toughness of polystyrene–poly(2-vinylpyridine) (PS–PVP) interfaces reinforced with PS–PVP diblock copolymers increased markedly when the molecular weight of both blocks exceeded M_c .²⁸ Similar effects have been observed for ductility. As shown in Figure 16a, the elongation at failure for monodisperse PS rises sharply above $M_n = 60$ kg/mol.²⁹ This value lies just above the critical molecular weight ($M_c = 31$ kg/mol) for this polymer.³⁰ The above generalization only holds for glassy polymers. Observe how hydrogenated polybutadiene (HPB) exhibits low ductility well beyond $M_c = 2.9$ kg/mol (Figure 16b).^{31,32} Its transition to highly ductile behavior does not occur until $M_n = 50$ kg/mol. Previous studies have found that the tensile strength, ductility, and fracture toughness of HPB all go through an abrupt transition over the same range.^{33,34} The value of 50 kg/mol, while not related to entanglement formation, corresponds to an important microstructural parameter. It corresponds to the point at which the root-mean-square end-to-end length of the chains (R) is roughly equal to the long period of the crystallites ($L \approx 14$ nm). In other words, the chain dimensions are just large enough to span the distance between two crystallites.

The significance of this observation is that the formation of intercrystalline linkages is the main criterion for the strong cohesive strength of PE. While entanglements may play a role in semicrystalline polymers with a glassy matrix, they do not appear to reinforce ones with a rubbery amorphous phase. Whether this observation can be extended to explain the current data is

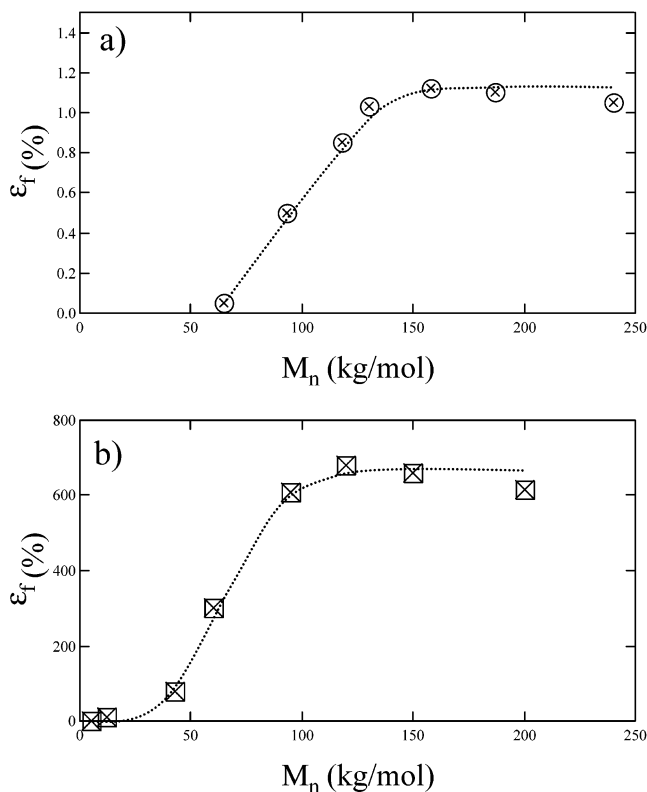


Figure 16. (a) Plot of elongation to failure vs number-average molecular weight for anionically polymerized polystyrene.²⁹ The strain to failure increases abruptly near 60 kg/mol. (b) Plot of elongation to failure vs weight-average molecular weight for hydrogenated polybutadiene.³¹ The strain to failure increases abruptly around 50 kg/mol. The dotted lines are guides to the eye.

unclear. It appears, however, that the transition to tough interfaces in the current study occurs between 30 and 85 kg/mol. This range agrees with the value of 50 kg/mol found for the onset of extensive plastic deformation in this polymer. If glassy polymer blocks need to double the entanglement molecular weight (M_e) to avoid entanglement slippage during craze breakdown, then perhaps semicrystalline blocks must participate in at least two crystallites to avoid the slippage of chains through the crystals.¹⁶

Tanzer et al. have studied the large strain deformation of HPB on a molecular level.³¹ By measuring the radius of gyration (R_g) of deuterium-labeled chains both before and after deformation, they were able to track how such chains responded to macroscopic deformation as a function of molecular weight. What they found was that chains smaller than 50 kg/mol deformed less than half as much as the bulk material. Chains larger than 50 kg/mol deformed more than the bulk material. To explain this observation, they hypothesized that the deformation of shorter chains could relax because of the lack of intercrystalline linkages. Portions of the chains participating in the amorphous phase would be able to return to their original random coil conformation shortly after the deformation. Longer chains, on the other hand, deform both by intracrystalline and intercrystalline shear. The latter process provides mechanical connectivity among neighboring crystallites and makes such large strains possible. It also prevents long-range relaxation of individual chains.

Such a mechanism would also hold for diblock copolymer reinforcement of an interface. While participation

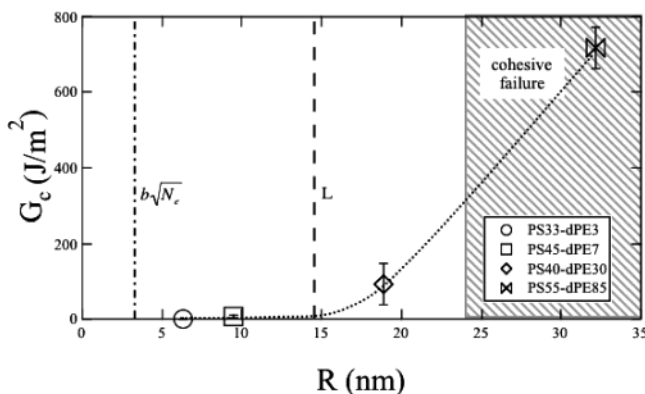


Figure 17. Fracture energy plotted vs the RMS end-to-end length of PE blocks for each diblock copolymer at a constant areal chain density of 0.2 chains/nm². Circles represent PS33-dPE3 copolymer, squares represent PS45-dPE7 copolymer, diamonds represent PS40-dPE 30 copolymer, and bowties represent PS50-dPE85 copolymer. The distance corresponding to the melt tube diameter is given by the dashed–dotted line, where b is the statistical segment length and N_e is the degree of polymerization between entanglements, and the distance corresponding to the long period of the lamellae is given by the dashed line. The dotted line is a guide to the eye.

in at least one crystallite is sufficient to produce intracrystalline shear, this deformation alone would not result in large-scale deformation and dissipation. The development of a large plastic zone would require the rotation and translation of different crystallites with respect to each other. This type of deformation could only be accomplished using semicrystalline blocks large enough to bridge two or more crystallites.

Figure 17 plots G_c as a function of the root-mean-square end-to-end distance (R) with the Σ held constant at 0.2 chains/nm². Notice that G_c does not become appreciable until R exceeds L . Despite the relatively low number of data points, the importance of the entanglement molecular weight of PE as a critical parameter can be ruled out. Furthermore, the change in molecular fracture mechanism from pullout to scission also appears to be unaffected by the entanglement molecular weight. This transition occurs somewhere between 30 and 85 kg/mol for the PE block. Additional molecular weights would need to be tested in order to more accurately determine the transition point.

Processing Effects. As stated in the Introduction, the ability to modify the mechanical properties of semicrystalline polymers through thermomechanical processing is one of their most important features. This feature ultimately arises from the dependence of those properties on the crystalline microstructure of the material. In the previous section, it was hypothesized that the long period of the crystallites plays an important role in the high strain properties of this material.

Table 3 shows the effects of cooling time on the PE microstructure. The SAXS data indicate an increase in the long period from 14.6 to 15.9 nm. In qualitative agreement with this observation is the change in microstructure seen in the TEM micrographs in Figure 10. Here we see a noticeable coarsening of the microstructure in going from a 2.7 min to a 3600 min cooling time. Although the shrinkage of the samples due to RuO₄ staining does not allow for a quantitative comparison, the micrographs do show that the lamellae become further spaced and more distinct with increasing cooling time.

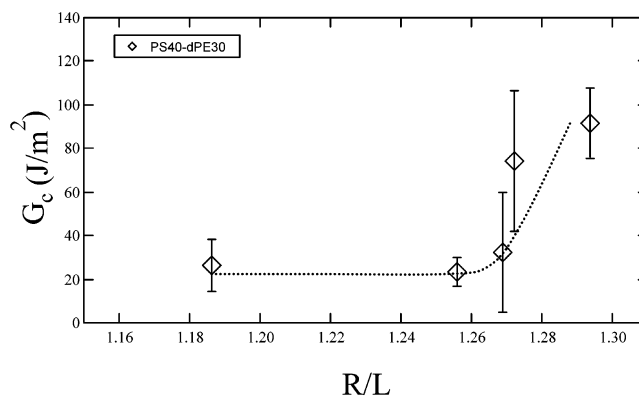


Figure 18. Fracture energy plotted as a function of the RMS end-to-end length of the PE block normalized to the lamellar long period. The dotted line is a guide to the eye.

Since the actual increase in L is so small, the relatively large change in G_c for the PS40-dPE30 copolymer is surprising. The plot of G_c vs R/L in Figure 18 shows a 4-fold increase in G_c due to the coarsening of the microstructure. This behavior not only supports the notion that the critical molecular weight for strong reinforcement is controlled by L , but it also suggests that this critical molecular weight lies near 30 kg/mol for this grade of PE.

Rate Dependence. One feature that distinguishes this system from the glassy ones studied previously is the sensitivity of the fracture energy to the crack growth rate. Increases as high as 250 J/m² were observed for a change in da/dt by 2 orders of magnitude. Such increases might be accounted for by viscoelastic behavior. In this case the viscoelastic dissipation would be expected to increase with increasing rate. According to the time–temperature superposition principle, faster rates bring the temperature of the experiment closer to the T_g of PE, thereby increasing the viscoelastic loss. A major flaw in this argument is that rate sensitivity was not observed for samples that failed cohesively. For these samples, the measured G_c involved only the bulk properties of the material. The lack of rate dependence implies that properties such as the loss modulus and crazing stress are constant over the range of da/dt tested. Further evidence can be seen in the lack of temperature dependence in Figure 13.

The only remaining possibility is that the stress transfer across the interface is a function of da/dt . It appears to be most sensitive when the chains fail by pullout. This tendency is illustrated in Figure 11, where the G_c of the low molecular weight copolymers scale with $(da/dt)^{0.4}$. As described earlier, only the first three data points for the PS40-dPE30 copolymer obey this 0.4 power law relationship. The last two points belong to a different scaling regime. Coinciding with the change in scaling is the appearance of deuterium on the PE fracture surface. This rise in deuterium level corresponds to a transition from pullout to scission beyond a crack growth rate of about 100 $\mu\text{m/s}$. Since the force to break a carbon–carbon bond does not change markedly with rate over this small range, the rate dependence of G_c should decrease as more chains fail by scission. Supporting this argument is the complete lack of rate sensitivity for the PS50-dPE85 samples, which were dominated by chain scission.

The proportionality of G_c with $(da/dt)^{0.4}$ can be linked to the rate dependence of the interfacial stress transfer through Brown's model for craze failure.³⁵ In his seminal

paper, Brown described how a stress concentration arises at the crack tip because of the low, but significant, shear modulus (C_{12}) of the craze. The finite shear modulus allows the craze material behind the crack to transmit load forward to the crack tip. The wider the craze is, the greater the amount of material that can intensify the stress concentration. The crack grows when the stress at the crack tip is equal to the stress needed to break the craze fibrils in this region (σ_f). In the limit that the craze width is much larger than the craze fibril spacing (d), G_c reduces to the following expression:

$$G_c = \frac{\pi d(1 - \nu_f)}{1.44\sqrt{C_{12}/C_{22}}\sigma_c} \sigma_f^2 \quad (5)$$

where ν_f is the volume fraction of polymer in the craze, and C_{22} is the tensile modulus of the craze material. Noting that craze fibrils fail directly at the interface, this equation demonstrates that stress transferred by the copolymer chains (σ_f) is the limiting factor for the development of G_c .

Since $G_c \propto \sigma_f^2$ and $G_c \propto (da/dt)^{0.4}$ the force transferred by individual chains should scale as $(da/dt)^{0.2}$. As simple viscous flow would give a linear relationship with da/dt , the observed dependence is not likely due to chain friction in the rubbery, amorphous phase. From the evidence considered in the previous two sections, diblock copolymer reinforcement appears to occur largely through the crystalline phase. The fact that the chains remain intact after fracture suggests that some sort of yield process is required to remove the PE blocks that have cocrystallized with the homopolymer. The rate dependence of the fracture energy, as a consequence, must arise from the deformation of crystallites in the interfacial region. The molecular basis for this dependence is difficult to analyze in terms of a yield stress. What would be expected is that greater resistance to crystalline yield would provide greater resistance to pullout and higher fracture energies.

Several theories have been proposed to explain the rate and temperature dependence of solid-state deformation in semicrystalline polymers. The most popular involve dislocation motion^{36–38} and melting/recrystallization.^{39–41} While both can account for many phenomena involved in deformation, they fail to explain important observations. The main weakness of the dislocation model is that the predicted temperature dependence of the yield stress is much weaker than that observed experimentally.⁴² The melting/recrystallization hypothesis, on the other hand, incorrectly predicts that the highest draw ratios should be achieved at the lowest strain rates. More recently, the α -relaxation process has been used to correctly account for both of the above behaviors.⁴³ The α -relaxation process refers to the helical motions of polymer chains within their crystals. It is a thermally activated process that participates in diffusion. Although it is responsible for a viscoelastic transition at the α -relaxation temperature, this motion occurs at all temperatures below the melting point.

The difficulty in assigning any of the above mechanisms to the present system is that the fracture energy in Figure 13 did not exhibit any temperature dependence. Although the range of temperatures tested was only 40 K, a decrease in G_c with increasing temperature would be predicted by all three of the above mechanisms. What seems apparent from the data is that the

underlying mechanism is either weakly dependent upon temperature, or not at all. It is instructive to note that, in going from 295 to 333 K, the temperature of the experiment only increased by a factor of 1.1. The crack growth rate, for comparison, increased by a factor of 110. While neither temperature nor da/dt were increased dramatically, the two effects should ultimately be correlated. More experiments would be needed in order to understand this discrepancy, and to determine the molecular basis for the $(da/dt)^{0.2}$ dependence of the pullout stress.

Conclusions

Unlike the PS–PVP system, PS–PE diblock copolymers are more likely to fail by chain pullout during craze breakdown. Forces less than that required for scission are sufficient to support wide crazes because of the lower crazing stress. In addition to the appearance of deuterium on the PS fracture surface, the decrease in Σ^\dagger with increasing M_n was also strong evidence for pullout. This phenomenon results from the increase in the frictional force per chain with increasing molecular weight.

The amorphous portion of PE appears to have little influence on the mechanical properties of its interface with PS. The primary evidence for this assertion is the notable absence of the entanglement molecular weight as a critical parameter. We observe that the strength of the interface does not improve dramatically until the PE block is 30 times longer than the entanglement molecular weight. The major transitions depend instead on the crystalline microstructure. Support for this notion is derived from the fact that the molecular weight transition corresponded to the point where $R > L$. Further evidence is provided by the decrease in G_c with increasing L near the critical molecular weight.

Also in contrast to glassy polymer–polymer interfaces, the current system exhibited significant rate dependence. Although the bulk properties were constant over the range of da/dt tested, G_c scaled with $(da/dt)^{0.4}$ when the chains failed by pullout. The G_c dependence decreased or ceased altogether when an increasing fraction of chains failed by scission. The lack of temperature dependence for G_c makes it difficult to determine the molecular deformation mechanism, but it is most likely related to a crystalline yield process.

Acknowledgment. This work was supported by the MRSEC Program of the National Science Foundation under Award No. DMR00-80034. J.J.B. thanks the U. C. Regents for fellowship support. P.F. acknowledges the support of the Internships in Nanosystems Science, Engineering and Technology program of the California NanoSystems Institute. We also thank Ken Cook from Exxon Corp. for his assistance in providing the PE films. Special thanks are extended to Jingjing Xu and Todd Jones from the University of Minnesota for their training in anionic synthesis techniques. We thank Frank Bates from the University of Minnesota as well for allowing us access to his facilities and for providing us with training. We also thank Gui Bazan and Zachary Komon for the use of their high-pressure reaction vessel.

References and Notes

- (1) Karger-Kocsis, J. *Mod. Plast.* **2002**, 79, 26.
- (2) Bunn, C. W. *Chemical Crystallography*; Oxford University Press: Oxford, England, 1945; p 233.

- (3) Voigt-Martin, I. G.; Alamo, R.; Mandelkern, L. *J. Polym. Sci., Part B: Polym. Phys.* **1986**, *24*, 1283.
- (4) Stehling, F. C.; Mandelkern, L. *Macromolecules* **1970**, *3*, 242.
- (5) Hendra, P. J.; Jobic, H. P.; Holland-Moritz, K. *J. Polym. Sci., Polym. Lett. Ed.* **1975**, *13*, 365.
- (6) Fakirov, S.; Krasteva, B. *J. Macromol. Sci.—Phys.* **2000**, *B39* (2), 297.
- (7) Morton, M.; Fetters, L. J. *Rubber Chem. Technol.* **1975**, *48*, 359.
- (8) Weimann, P. A.; Jones, T. D.; Hillmyer, M. A.; Bates, F. S.; Londono, J. D.; Melnichenko, Y.; Wignall, G. D.; Almdal, K. *Macromolecules* **1997**, *30*, 3650.
- (9) Bideaux, J.-E.; Smith, G. D.; Bernet, N.; Manson, J.-A. E.; Hilborn, J. *Polymer* **1996**, *37*, 1129.
- (10) Boucher, E.; Folkers, J. P.; Hervet, H.; Léger, L.; Creton, C. *Macromolecules* **1996**, *29*, 774.
- (11) Boucher, E.; Folkers, J. P.; Creton, C.; Hervet, H.; Léger, L. *Macromolecules* **1997**, *30*, 2102.
- (12) Plummer, C. J. G.; Kausch, H.-H.; Creton, C.; Kalb, F.; Léger, L. *Macromolecules* **1998**, *31*, 6164.
- (13) Kalb, F.; Léger, L.; Creton, C.; Plummer, J. G.; Marcus, P.; Malgalhaes, A. *Macromolecules* **2001**, *34*, 2702.
- (14) Hermes, H. E.; Bucknall, D. G.; Higgins, J. S.; Scherrenberg, R. L. *Polymer* **1998**, *39*, 3099.
- (15) Duchet, J.; Chapel, J.-P.; Chabert, B.; Gerard, J.-F. *Macromolecules* **1998**, *31*, 8264.
- (16) Washiyama, J.; Creton, C.; Kramer, E. J.; Xiao, F.; Hui, C.-Y. *Macromolecules* **1993**, *26*, 6011.
- (17) Creton, C.; Kramer, E. J.; Hui, C.-Y.; Brown, H. R. *Macromolecules* **1990**, *24*, 1846.
- (18) Washiyama, J.; Creton, C.; Kramer, E. J.; Xiao, F.; Hui, C.-Y. *Macromolecules* **1994**, *27*, 2019.
- (19) Mandelkern, L. *Polym. J.* **1985**, *17*, 337.
- (20) Mandelkern, L. *Discuss. Faraday Soc.* **1979**, *68*, 310.
- (21) Chaffin, K. A.; Bates, F. S.; Brant, P.; Brown, G. M. *J. Polym. Sci., Part B: Polym. Phys.* **2000**, *38*, 108.
- (22) Gilman, H.; Cartledge, F. K. *J. Organomet. Chem.* **1964**, *2*, 447.
- (23) Hutchinson, J. W.; Suo, Z. *Adv. Appl. Mech.* **1991**, *29*, 63.
- (24) Nairn, J. A. *Int. J. Adhes. Adhes.* **2000**, *20*, 59.
- (25) Feldman, L. C.; Mayer, J. W. In *Fundamentals of Surface and Thin Film Analyses*; North-Holland: Amsterdam, 1986.
- (26) Mills, P. J.; Green, P. F.; Palmstrom, C. J.; Mayer, J. W.; Kramer, E. J. *J. Appl. Phys. Lett.* **1984**, *45*, 958.
- (27) Quinn, F. A.; Mandelkern, L. *J. Am. Chem. Soc.* **1958**, *80*, 3178.
- (28) Kramer, E. J.; Norton, L. J.; Dai, C.-A.; Sha, Y.; Hui, C.-Y. *Faraday Discuss.* **1994**, *98*, 31.
- (29) Martin, J. R.; Johnson, J. F.; Cooper, A. R. *J. Macromol. Sci. (C)* **1972**, *8*, 57.
- (30) Fetters, L. J.; Lohse, D. J.; Milner, S. T.; Graessley, W. W. *Macromolecules* **1999**, *32*, 6847.
- (31) Tanzer, J. D.; Crist, B.; Graessley, W. W. *J. Polym. Sci., Part B: Polym. Phys.* **1989**, *27*, 859.
- (32) Fetters, L. J.; Lohse, D. J.; Richter, T. A.; Witten, T. A.; Zirkel, A. *Macromolecules* **1994**, *27*, 4639.
- (33) Fisher, C. J. M.S. Thesis, Northwestern University, 1985.
- (34) Fulmer, G. E.; Horowitz, R. H. *Proceedings of the 7th International Congress of Rheology*; Gothenburg, 1976; p 624.
- (35) Brown, H. R. *Macromolecules* **1991**, *24*, 2757.
- (36) Young, R. J. *Mater. Forum* **1988**, *11*, 210.
- (37) Crist, B.; Fischer, C. J.; Howard, P. R. *Macromolecules* **1989**, *22*, 1709.
- (38) Crist, B. *Polym. Commun.* **1989**, *30*, 69.
- (39) Flory, P. J.; Yoon, D. Y. *Nature (London)* **1978**, *272*, 226.
- (40) Wignall, G. D.; Wu, W. *Polym. Commun.* **1983**, *24*, 354.
- (41) Wu, W.; Wignall, G. D.; Mandelkern, L. *Polymer* **1992**, *33*, 4137.
- (42) Peacock, A. J.; Mandelkern, L.; Alamo, R. G.; Fatou, J. G. *J. Mater. Sci.* **1998**, *33*, 2255.
- (43) Hu, W.-G.; Schmidt-Rohr, K. *Acta Polym.* **1999**, *50*, 271.

MA034013J